Intrinsic point defects and complexes in the quaternary kesterite semiconductor Cu_2ZnSnS_4

Shiyou Chen,[1,2] Ji-Hui Yang,[1] X. G. Gong,[1] Aron Walsh,[3] and Su-Huai Wei[4]

[1]*Key Laboratory for Computational Physical Sciences (MOE) and Surface Physics Laboratory, Fudan University, Shanghai 200433, China*

[2]*Laboratory of Polar Materials and Devices, East China Normal University, Shanghai 200241, China*

[3]*Department of Chemistry, University College London, London WC1E 6BT, United Kingdom*

[4]*National Renewable Energy Laboratory, Golden, Colorado 80401, USA*

(Received 8 April 2010; revised manuscript received 10 May 2010; published 8 June 2010)

Current knowledge of the intrinsic defect properties of Cu_2ZnSnS_4 (CZTS) is limited, which is hindering further improvement of the performance of CZTS-based solar cells. Here, we have performed first-principles calculations for a series of intrinsic defects and defect complexes in CZTS, from which we have the following observations. (i) It is important to control the elemental chemical potentials during crystal growth to avoid the formation of secondary phases such as ZnS, CuS, and Cu_2SnS_3. (ii) The intrinsic *p*-type conductivity is attributed to the Cu_{Zn} antisite which has a lower formation energy and relatively deeper acceptor level compared to the Cu vacancy. (iii) The low formation energy of many of the acceptor defects will lead to the intrinsic *p*-type character, i.e., *n*-type doping is very difficult in this system. (iv) The role of electrically neutral defect complexes is predicted to be important, because they have remarkably low formation energies and electronically passivate deep levels in the band gap. For example, $[Cu_{Zn}^{-}+Zn_{Cu}^{+}]$, $[V_{Cu}^{-}+Zn_{Cu}^{+}]$, and $[Zn_{Sn}^{2-}+2Zn_{Cu}^{+}]$ may form easily in nonstoichiometric samples. The band alignment between Cu_2ZnSnS_4, $CuInSe_2$ and the solar-cell window layer CdS has also been calculated, revealing that a type-II band alignment exists for the CdS/Cu_2ZnSnS_4 heterojunction. The fundamental differences between CZTS and $CuInSe_2$ for use in thin-film photovoltaics are discussed. The results are expected to be relevant to other I_2-II-IV-VI_4 semiconductors.

DOI: 10.1103/PhysRevB.81.245204 PACS number(s): 61.72.J−, 61.50.Ah, 71.20.Nr, 71.55.Gs

I. INTRODUCTION

The quaternary Cu_2ZnSnS_4 (CZTS) semiconductor has drawn an increasing amount of attention recently[1–7] because it is a strong candidate low-cost thin-film solar-cell absorber material with the optimal single-junction band gap (~1.5 eV) and a high adsorption coefficient ($>10^4$ cm^{-1}).[8–11] Unlike the ternary $CuInSe_2$- and binary CdTe-based solar cells, all the constituent elements in Cu_2ZnSnS_4 are naturally abundant and nontoxic. Cu_2ZnSnS_4 can be derived from $CuInS_2$ through replacing two In atoms by one Zn and one Sn, crystallizing in the kesterite structure (space group $I\bar{4}$).[12–14] The light to electricity conversion efficiency of Cu_2ZnSnS_4-based solar cells has increased from 0.66% in 1996 to almost 10% in 2010.[9,15,16]

Despite the increase in the efficiency, the detailed physical properties of this semiconductor absorber are still far from clear, which has hindered further efficiency improvement.[9] For example, it is well known that the *p*-type self-doping in $CuInSe_2$ is due to Cu vacancy[17–19] and the related defect physics has been widely studied and explained.[19,20] However, until recently[21–23] no experimental or theoretical work had been done to clarify what defects contribute to the widely observed *p*-type conductivity in Cu_2ZnSnS_4.[1,8,10,24–31] Since the bonding character, crystal, and electronic structure are similar for Cu_2ZnSnS_4 and $CuInSe_2$, it is natural to know if the Cu vacancy is also the dominant defect in Cu_2ZnSnS_4.

Furthermore, one of the important factors that leads to high efficiency of the $CuIn_{1-x}Ga_xSe_2$ solar cells, despite having poor crystallinity, is that intrinsic defects in $CuInSe_2$ undergo self-passivation, e.g., forming the $[In_{Cu}^{2+}+2V_{Cu}^{-}]$ complex,[17] and the interface between the $CuInSe_2$ absorber layer and the CdS window layer can be type inverted to become *n*-type, which facilitates the separation of the electron-hole pairs. However, this electrically benign character disappears in the wider-gap $CuGaSe_2$ (1.68 eV), because of the deep Ga_{Cu} donor level forms an electron trap,[19] pinning the Fermi level and resulting in the *n*-type doping difficulty.[32,33] This restriction has limited the further improvement of the solar-cell efficiency through alloying more Ga in $CuIn_{1-x}Ga_xSe_2$ to increase the band gap and thus the open-circuit voltage. According to experimental observation, the $CuIn_{1-x}Ga_xSe_2$ solar cell with the highest efficiency has an absorber band gap less than 1.2 eV,[34] lower than the optimal band gap (1.4–1.5 eV) for single-junction cell. As a candidate for replacing $CuIn_{1-x}Ga_xSe_2$, Cu_2ZnSnS_4 has a relatively wide band gap (~1.5 eV), closer to the value of $CuGaSe_2$ (1.7 eV), therefore it is important to know if Cu_2ZnSnS_4 can be doped *n* type easily and if its defect properties give the similar electrically benign character as $CuInSe_2$.

To address these questions, we have performed first-principles theoretical calculations of the formation-energy and the transition-energy levels for a series of intrinsic point defects and defect complexes in Cu_2ZnSnS_4. Because the formation of intrinsic defects is related directly to the nonstoichiometry of the samples and to the formation of secondary phases, our study also gives hints for the crystal growth in controlling the elemental environment, to produce good-quality stoichiometric crystals and to avoid the secondary phases such as ZnS, Cu_2SnS_3, or compositional nonuniformity,[8,9,11,15,25,35–37] which are still challenges in the

 ©2010 The American Physical Society

preparation of high-quality single-phase quaternary compounds.

In a recent letter,[21] we communicated our initial results of intrinsic defect formation in CZTS. Due to the importance of this subject and the complexity of the underlying defect physics, in this paper we present a comprehensive analysis based on further calculations and show that: (i) the atomic chemical potentials that stabilize this quaternary compound are limited to a very narrow range by the secondary phases CuS, Cu_2S, ZnS, SnS, Cu_2SnS_3, etc. (ii) In the stable crystal, the Cu_{Zn} antisite contributes mostly to the *p*-type conductivity, different from $CuInSe_2$ where the Cu vacancy dominates, and the transition energy level of this antisite is relatively deeper than V_{Cu}. (iii) *n*-type doping of this quaternary kesterite material should be difficult due to the facile formation of compensating acceptor defects, which can be understood through the same Fermi-level pinning mechanism established for $CuInSe_2$ and $CuGaSe_2$. (iv) The band alignment for CdS/Cu_2ZnSnS_4 is type II, which facilitates electron-hole separation. (v) Electrically benign defect character is possible in this system due to the charge compensation of various defect complexes in the cation sublattice.

II. CALCULATION METHODS

A. Defect formation

To calculate the defect formation-energy $\Delta H(\alpha,q)$ and transition-energy levels $\epsilon(\alpha,q/q')$, we use the supercell approach in which a defect α in the charge state q is placed in a 64-atom Cu_2ZnSnS_4 supercell. From the total energy $E(\alpha,q)$ of the supercell with a defect and that of the perfect supercell $E(host)$, we deduce $\Delta H(\alpha,q)$ according to[17,38]

$$\Delta H(\alpha,q) = E(\alpha,q) - E(host) + \sum_i n_i(E_i + \mu_i) + q[\epsilon_{\rm VBM}(host) + E_F], \quad (1)$$

where μ_i is the atomic chemical potential of constituent i referenced to the total energy E_i of its pure elemental solid, e.g., face-centered-cubic (fcc) Cu, Zn, and α-Sn. $\mu_i=0$ represents the limit where the element is so rich that their pure solid phase can form. E_F is the Fermi energy level referenced to the valence-band maximum (VBM) of the host Cu_2ZnSnS_4. n_i is the number of atom i and q is the number of electrons exchanged between the supercell and the corresponding thermodynamic reservoir in forming the defect, e.g., for the negatively charged Cu_{Zn} antisite (Cu_{Zn},−1), $n_{Cu}=-1$, $n_{Zn}=1$, and $q=-1$.

The defect transition-energy level $\epsilon_\alpha(q/q')$ is defined as the Fermi energy level at which the formation energy $\Delta H(\alpha,q)$ of the α defect with charge q is equal to $\Delta H(\alpha,q')$ with a different charge q', i.e., this represents the adiabatic transition energy between two defect charge states. More information about the defect methodology adopted is described in Refs. 17 and 38.

The total energy and band structure are calculated within the density-functional formalism as implemented in the VASP code.[39] For the exchange-correlation potential, we used the generalized gradient approximation (GGA) of Perdew and Wang, known as PW91.[40] The frozen-core projector augmented-wave potentials[41] were employed with an energy cutoff of 300 eV for plane waves and a $2\times2\times2$ Monkhorst-Pack *k*-point mesh to give converged results. A supercell size as large as 128 atom was also used to test the convergence of the formation energy, showing that the formation energy change for V_{Cu}, V_{Zn}, and Zn_{Cu} are less than 0.03 eV from the result of 64-atom supercell. The estimated error is 0.1 eV for the calculated formation energies and the transition-energy levels.[17]

The difference between the calculated and experimental band gap of CZTS is corrected through a rigid shift of the conduction band with the donor levels shifted upward correspondingly, as described in Ref. 17. To test the influence of this band-gap correction, we have performed additional calculations using a nonlocal hybrid functional [HSE06 (Refs. 42 and 43)], where 25% of the semilocal GGA exchange potential is replaced by screened Fock exchange. The HSE06 functional reproduces the experimental band gap of CZTS,[12] albeit at larger computational expense. At this level of theory, the formation energy of the Zn_{Cu} donor is about 0.1 eV higher than the value obtained by the simple rigid band correction.

It should be noted that in the kesterite structure, there are two crystallographically distinct Cu sites (2*a* and 2*c* Wyckoff positions).[10,44] As the local coordination is the same and the sites only differ in their long-range environment, the formation-energy difference for defects at the two sites is small (<0.02 eV). The lowest energy configurations are reported for both isolated point defects and defect complexes.

B. Band alignment

The valence-band offset $\Delta E_v(A/B)$ between A and B is calculated following the same procedure as in core-level photoemission measurements.[45–47] We first calculate the energy-level difference between VBM and the core levels for A and B, i.e., $\Delta E^{\rm A}_{\rm VBM,C}$ and $\Delta E^{\rm B}_{\rm VBM',C'}$, respectively, then we form a superlattice for A and B, and calculate the core-level difference $\Delta E_{\rm C',C}$ between A and B. When A is kesterite Cu_2ZnSnS_4 and B is chalcopyrite $CuInSe_2$, a (001) superlattice with four-cation-layer A and four-cation-layer B alternatively is used to make the local charge-neutrality condition always satisfied and gives reliable results. The valence-band offset $\Delta E_v(A/B)$ can then be derived by

$$\Delta E_v(A/B) = \Delta E^{\rm B}_{\rm VBM',C'} - \Delta E^{\rm A}_{\rm VBM,C} + \Delta E_{\rm C',C} \quad (2)$$

and the conduction-band offset $\Delta E_c(A/B)$ is deduced as

$$\Delta E_c(A/B) = \Delta E_v(A/B) + \Delta E_g(A/B), \quad (3)$$

where ΔE_g is the experimentally measured band-gap difference of A and B.

III. STABLE REGION IN CHEMICAL-POTENTIAL SPACE

From Eq. (1), it can be seen that the defect formation energy depends on the atomic chemical potential, which is thermodynamically limited by several conditions. First, since $\mu_{Cu}=0$ means Cu is rich enough to form the pure fcc metal,

to avoid this phase when synthesizing Cu_2ZnSnS_4 it is required that $\mu_{Cu}<0$ and similarly $\mu_{Zn}<0$, $\mu_{Sn}<0$, and $\mu_S<0$. Second, to maintain a stable Cu_2ZnSnS_4 crystal, the chemical potential of Cu, Zn, Sn, and S must satisfies the following equation:

$$2\mu_{Cu}+\mu_{Zn}+\mu_{Sn}+4\mu_S=\Delta H_f(Cu_2ZnSnS_4), \quad (4)$$

where $\Delta H_f(Cu_2ZnSnS_4)=-4.21$ eV is the calculated formation enthalpy of the Cu_2ZnSnS_4. Third, to avoid the formation of secondary phases such as CuS, Cu_2S, ZnS, SnS, SnS_2, and Cu_2SnS_3, the following relations must be satisfied:

$$\mu_{Cu}+\mu_S<\Delta H_f(CuS)=-0.49 \text{ eV},$$

$$2\mu_{Cu}+\mu_S<\Delta H_f(Cu_2S)=-0.52 \text{ eV},$$

$$\mu_{Zn}+\mu_S<\Delta H_f(ZnS)=-1.75 \text{ eV},$$

$$\mu_{Sn}+\mu_S<\Delta H_f(SnS)=-1.01 \text{ eV},$$

$$\mu_{Sn}+2\mu_S<\Delta H_f(SnS_2)=-1.33 \text{ eV},$$

$$2\mu_{Cu}+\mu_{Sn}+3\mu_S<\Delta H_f(Cu_2SnS_3)=-2.36 \text{ eV}, \quad (5)$$

where $\Delta H_f(CuS)$, $\Delta H_f(Cu_2S)$, $\Delta H_f(ZnS)$, $\Delta H_f(SnS)$, $\Delta H_f(SnS_2)$, and $\Delta H_f(Cu_2SnS_3)$ are the calculated formation enthalpies of binary and ternary compounds. The crystal structure of these compounds are CuS (covellite structure, space group $P6_3/mmc$), Cu_2S (low chalcocite structure, $P21/c$), ZnS (zinc blende, $F\bar{4}3m$), SnS (quasitetragonal distorted rocksalt structure, $Pnma$),[48] SnS_2 (berndtite structure, $P\bar{3}m1$), and Cu_2SnS_3 (a sphalerite-type superstructure, space group Cc).[49] Since $\Delta H_f(Cu_2ZnSnS_4)-\Delta H_f(Cu_2S)-\Delta H_f(ZnS)-\Delta H_f(SnS_2)=-0.81$ eV<0 and $\Delta H_f(Cu_2ZnSnS_4)-2\Delta H_f(CuS)-\Delta H_f(ZnS)-\Delta H_f(SnS)=-0.47$ eV<0, the quarternary compound can be synthesized when $Cu_2S+ZnS+SnS_2$ and $2CuS+ZnS+SnS$ are mixed stoichiometrically under high temperature. In fact, these binary compounds are used as the starting materials for different synthesis procedures.[15,25,30,35,36,50,51]

Under the established constraints, the chemical-potential range of Cu, Zn, and Sn that stabilizes the Cu_2ZnSnS_4 compound is bound in a polyhedron in the three-dimensional $(\mu_{Cu},\mu_{Zn},\mu_{Sn})$ space. In Fig. 1 we plot the slices of the polyhedron in $\mu_{Cu}=0$ and -0.55 eV plane to show how the secondary phases limit the formation of Cu_2ZnSnS_4. The black area in Fig. 1(a) and the point **G** in Fig. 1(b) show the chemical-potential region which stabilizes Cu_2ZnSnS_4. These stable areas are surrounded by different lines, and on the other side of these lines, secondary phases (see the compound names labeled with the same color as the lines in Fig. 1) form. For example, in Fig. 1(a) ZnS will form inevitably when the chemical potential is Zn rich (e.g., $\mu_{Zn}>-0.9$ eV). The line corresponding to SnS_2 is not plotted in the $\mu_{Cu}=0$ slice [Fig. 1(a)], as it is far from the stable region (black) and thus do not have direct limit on the region. Figure 1(b) shows the slice in $\mu_{Cu}=-0.55$ eV plane, and the stable region here is, in fact, only a point **G** and a slight deviation of the chemical potential in this plane will produce ZnS or SnS_2 secondary phases, indicating that **G** is one of the end points of the three-dimensional stable polyhedron. It is not shown in Fig. 1, but our calculations show that μ_{Cu} is limited to the range between −0.55 and 0 eV, and the stable area becomes smaller and smaller as μ_{Cu} approaches −0.55 eV.

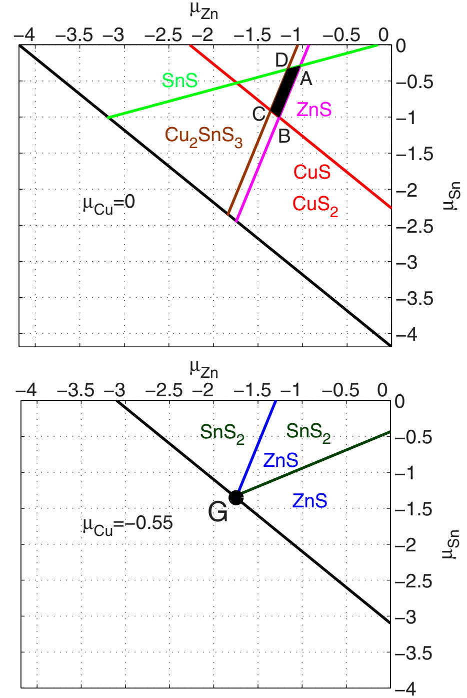

FIG. 1. (Color online) The calculated stable chemical-potential region of Cu_2ZnSnS_4 in the $\mu_{Cu}=0$ plane (a, the black area surrounded by **A**, **B**, **C**, and **D** points) and $\mu_{Cu}=-0.55$ eV plane (b, **G** point) of $(\mu_{Cu},\mu_{Zn},\mu_{Sn})$ space. All values are in eV. See the text for more information.

The narrow stable areas at different (μ_{Zn},μ_{Sn}) planes show that the chemical-potential control is very important for growing good-quality Cu_2ZnSnS_4 crystals. In particular, the stable area for μ_{Zn} is very slim, thus the content control of Zn should be taken very carefully. Comparing the three cations, μ_{Zn} (lower than −0.9 eV) has a relatively lower value than μ_{Cu} (between −0.55 and 0 eV) and μ_{Sn} (between −0.3 and −1.4 eV), which is due to the strong binding between Zn and S. Thus, perfect Cu_2ZnSnS_4 crystals are thermodynamically unstable when Zn is rich (near the $\mu_{Zn}=0$ plane). Experimentally, it is observed that under Cu-poor and Zn-rich conditions, compositional nonuniformity exists,[9,11,15,25,35,36] which should be related to the secondary phase segregation of ZnS.

IV. RESULTS AND DISCUSSION

A. Isolated point defects

In Table I, we show the calculated formation energy of isolated point defects such as vacancies, antisites, and interstitials at different chemical-potential points, **A**, **B**, **C**, **D**, **E**, **F**, and **G**, which are in the stable region of Cu_2ZnSnS_4. **A**, **B**, **C**, and **D** are in the $\mu_{Cu}=0$ plane (Cu-rich condition), as shown in Fig. 1, while from **E** to **F** to **G** μ_{Cu} becomes lower,

TABLE I. The formation energy $\Delta H(\alpha,0)$ (eV) of isolated point defects in Cu_2ZnSnS_4 at different chemical potentials **A**, **B**, **C**, **D** (shown in Fig. 1), **E**, **F**, and **G**.

Defect	V_{Cu}	V_{Zn}	V_{Sn}	Cu_{Zn}	Zn_{Cu}	Cu_{Sn}	Sn_{Cu}	Zn_{Sn}	Sn_{Zn}	Cu_i	Zn_i	Sn_i	V_S
Cu poor													
$\mu_{Cu}=-0.55$, $\mu_{Zn}=-1.75$, $\mu_{Sn}=-1.35$, $\mu_S=0$ (**G**)													
$\Delta H(\alpha,0)$	0.21	0.39	1.77	−0.16	2.60	0.37	7.05	0.36	4.44	3.68	6.65	9.17	1.71
$\mu_{Cu}=-0.40$, $\mu_{Zn}=-1.43$, $\mu_{Sn}=-0.71$, $\mu_S=-0.32$ (**F**)													
$\Delta H(\alpha,0)$	0.37	0.71	2.41	0.00	2.43	0.85	6.56	0.68	4.12	3.53	6.33	8.53	1.39
$\mu_{Cu}=-0.10$, $\mu_{Zn}=-1.13$, $\mu_{Sn}=-0.40$, $\mu_S=-0.62$ (**E**)													
$\Delta H(\alpha,0)$	0.67	1.02	2.72	0.01	2.43	0.87	6.54	0.69	4.11	3.23	6.02	8.22	1.09
Cu rich													
$\mu_{Cu}=0$, $\mu_{Zn}=-1.03$, $\mu_{Sn}=-0.29$, $\mu_S=-0.72$ (**A**)													
$\Delta H(\alpha,0)$	0.77	1.12	2.82	0.01	2.42	0.87	6.54	0.69	4.11	3.13	5.92	8.11	0.99
$\mu_{Cu}=0$, $\mu_{Zn}=-1.26$, $\mu_{Sn}=-1.00$, $\mu_S=-0.49$ (**B**)													
$\Delta H(\alpha,0)$	0.77	0.88	2.11	−0.23	2.66	0.16	7.25	0.22	4.58	3.13	6.16	8.83	1.23
$\mu_{Cu}=0$, $\mu_{Zn}=-1.36$, $\mu_{Sn}=-0.91$, $\mu_S=-0.49$ (**C**)													
$\Delta H(\alpha,0)$	0.77	0.79	2.21	−0.32	2.76	0.26	7.16	0.40	4.39	3.13	6.25	8.73	1.23
$\mu_{Cu}=0$, $\mu_{Zn}=-1.17$, $\mu_{Sn}=-0.34$, $\mu_S=-0.68$ (**D**)													
$\Delta H(\alpha,0)$	0.77	0.98	2.78	−0.13	2.57	0.83	6.59	0.79	4.01	3.13	6.06	8.16	1.04

and thus more Cu poor. A plot of the formation energy as a function of the chemical potential is shown in Fig. 2.

From these numbers, we can see that among all these intrinsic defects, Cu_{Zn}, Cu_{Sn}, Zn_{Sn}, V_{Cu}, and V_{Zn} have relatively low formation energy, lower than 1.0 eV at point **E**. Cu_{Zn} is the lowest-energy defect at all the points in the stable region, significantly lower than that of V_{Cu} and Zn_{Sn}, showing that the Cu_{Zn} antisite is the dominant intrinsic defect in this quaternary kesterite semiconductor, if secondary phases are avoided in the synthesis, different from the behavior of chalcopyrite $CuInSe_2$ where the Cu vacancy is the predominant defect. One difference between Cu_2ZnSnS_4 and $CuInSe_2$ is that the quaternary compound has three kinds of cations, giving more possible antisite defects, and when the size and valence difference of the antisite cations are small, such as Cu and Zn, the antisite Cu_{Zn} can have lower formation energy than Cu vacancy because the difference between Cu and Zn is smaller than Cu and a vacancy, while in ternary $CuInSe_2$ the large difference between Cu and In makes the antisite Cu_{In} have higher formation energy than V_{Cu}.

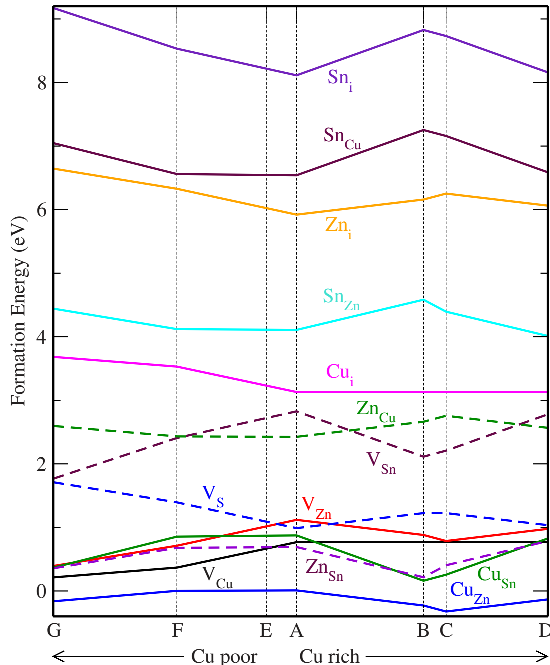

FIG. 2. (Color online) The formation energy of neutral intrinsic defects in Cu_2ZnSnS_4 as a function of the chemical potential at points **A**, **B**, **C**, **D**, **E**, **F**, and **G** shown in Fig. 1 and Table I.

It should be noted that the formation energy depends on the chemical potential according to Eq. (1). To avoid the ZnS secondary phase, μ_{Zn} is always lower than −0.9 eV at the seven points in Table I, which decreases the formation energy of Cu_{Zn} and V_{Zn} by more than −0.9 eV. Thus, the lower formation energy of Cu_{Zn} than V_{Cu} also reflects the low chemical potential of Zn in the stable region.

As we have mentioned, the equilibrium chemical-potential region stabilizing Cu_2ZnSnS_4 is limited by the competitive compounds in the synthesis, and outside the region these compounds may form as secondary phases. However, for compounds with a commensurate lattice, their creation can also be considered as the spontaneous formation of a large concentration of ordered intrinsic defects in Cu_2ZnSnS_4, reflected by the negative formation energy of the defect at that chemical potential. In other words, the stable region excludes the chemical-potential points where a certain kind of defect has a negative formation energy. In Fig. 1 we considered only six competitive compounds in determining the stable region, and there are many other binary, ternary, and even quaternary compounds constituting of

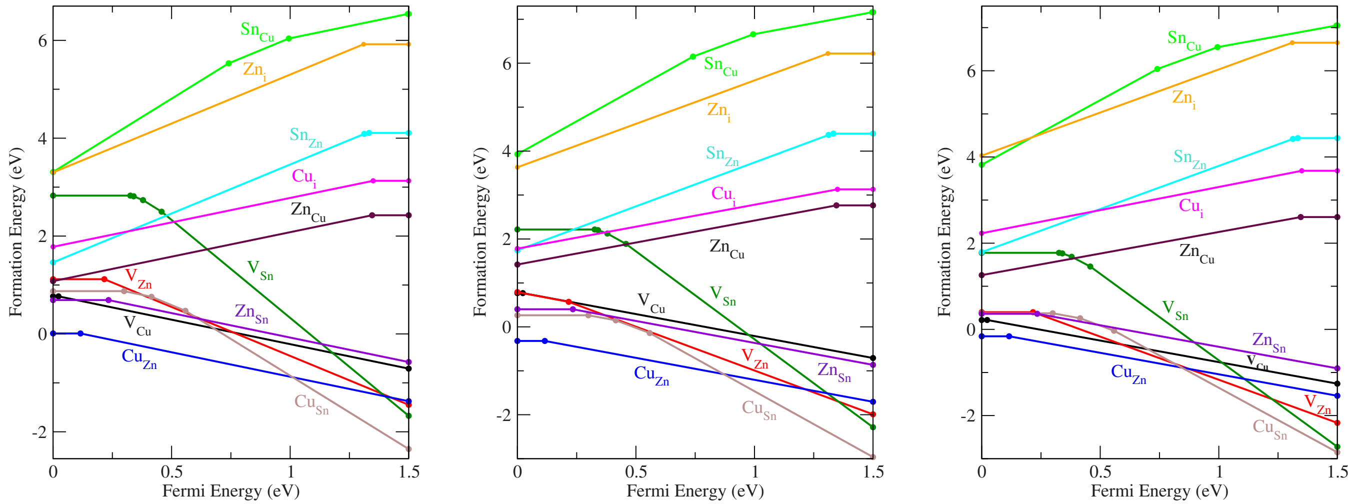

FIG. 3. (Color online) The change in the defect formation energy as a function of the Fermi energy at the chemical-potential points **A** (left), **C** (center), and **G** (right). For each value of E_F only the most stable charge state is plotted with the filled circles representing a change in charge state (transition energy level).

Cu, Zn, Sn, and S, which may have further limit on the stable region, shrinking it to a even smaller size. In Table I, it is shown that negative formation energies are found at certain chemical-potential points, e.g., at **G**, **B**, **C**, and **D** the formation energy of Cu_{Zn} is negative, indicating that at these chemical potentials Cu-rich secondary phases can exist. According to our calculation, the chemical-potential points that give positive formation energy for all these intrinsic defects are along the line **F**$\rightarrow$**E**$\rightarrow$**A**, and a deviation from this line causes off stoichiometry. In our previous letter,[21] the stable point **P** (μ_{Cu}=−0.20 eV, μ_{Zn}=−1.23 eV, and μ_{Sn}=−0.50 eV) is just at the middle point of the **F**$\rightarrow$**E**$\rightarrow$**A** line. The shrinking of the stable region to a line indicates again that the chemical-potential control is very important for synthesizing good-quality Cu_2ZnSnS_4 crystals. Zn should be poor enough to avoid ZnS secondary phase formation, but it should not be too poor to form a large amount of Zn vacancies and Cu_{Zn} antisite defects.

B. Transition-energy levels and intrinsic doping limits

According to Eq. (1), the formation energy of charged defects also depends on the Fermi energy level E_F, i.e., $\Delta H(\alpha,q)$ of negatively charged acceptors decreases as E_F shifts from the VBM to conduction-band minimum (CBM), while that of positively charged donors decreases as E_F shifts from CBM to VBM, as shown in Fig. 3. The turning points stand for the transition-energy levels at which defects with different charges have the same formation energy and the slope depends on the charge state.

The calculated transition-energy levels for all intrinsic defects are listed in Fig. 4. We look at the dominant defect Cu_{Zn} first, which has an $\epsilon(-/0)=0.12$ eV acceptor level above the VBM. However, the higher-energy V_{Cu} acceptor has a relatively shallower level at 0.02 eV above the VBM, as shallow as that in $CuInSe_2$(0.03 eV). The deeper level of Cu_{Zn} can be explained by considering that the Cu on Zn antisite enhances the p-d hybridization between Cu and S.[12] As shown in Fig. 5, the wave function of the acceptor level has the similar distribution character as the VBM state, localizing mainly around Cu and S, which indicates that the Cu_{Zn} accepter level has also the antibonding component of p-d hybridization between Cu and S, as the VBM state. The increased distribution on the atomic site of Cu_{Zn} antisite in Cu-S-Zn plane shows the replacement of Zn by Cu enhances this hybridization, pushing the antibonding level and thus the $\epsilon(-/0)$ level higher relative to the weakened hybridization introduced by the Cu vacancy. The other two low-energy defects at the chemical-potential point **A**, Cu_{Sn} and Zn_{Sn} have even deeper acceptor levels. It should be noted that both V_{Zn} and Zn_{Sn} are negative-U defects, with $\epsilon(2-/0)$ level shallower than $\epsilon(-/0)$, because a direct transition to the closed-shell −2 charge gains more energy. The acceptor levels related with higher valences are even deeper, close to the middle of the band gap, e.g., $\epsilon(4-/3-)$ of V_{Sn} and $\epsilon(3-/2-)$ of Cu_{Sn}.

On the donor side, $\epsilon(0/+)$ of low-energy donors Zn_{Cu} and Cu_i are about 0.15 eV below the CBM with the wave function of the donor state follows the character of the CBM

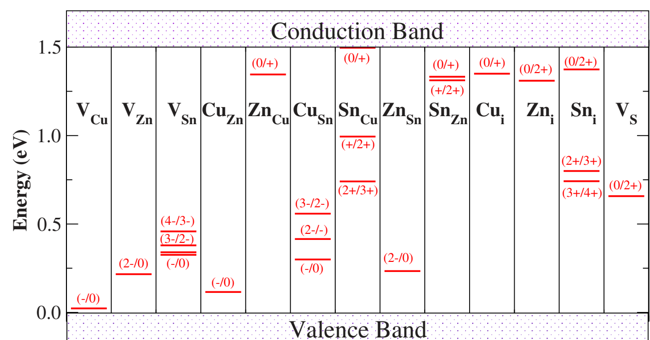

FIG. 4. (Color online) The transition-energy levels of intrinsic defects in the band gap of Cu_2ZnSnS_4. The GGA band gap is corrected to the experimental value 1.5 eV, and the donor levels are shifted together with the CBM level.

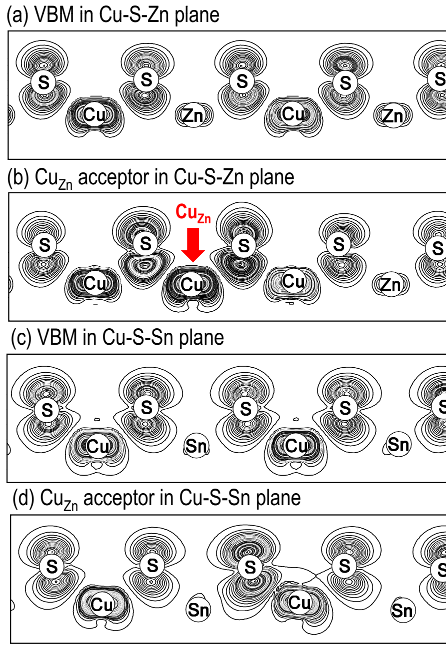

FIG. 5. (Color online) The contour plot of the charge density of the VBM state and Cu_{Zn} acceptor state in Cu-S-Zn and Cu-S-Sn planes, respectively. The red arrow shows the atomic site of the Cu_{Zn} antisite. The charge density is calculated as the squared norm of the one-particle wave function corresponding to the eigenvalues of the defect level or VBM level at Γ point.

state. As shown in Fig. 6, both Zn_{Cu} donor and CBM states are localized mainly around Sn and S sites, while the distribution on Cu and Zn are less and the change caused by the Zn on Cu antisite is also small, which is because both $\epsilon(0/+)$ donor and CBM states have the antibonding character of Sn and S *s*-*s* hybridization while the *s* levels of Cu and Zn are higher than that of Sn and thus has less component in this hybridization. It is interesting to see that the Sn_{Cu} donor level $\epsilon(0/+)$ is very shallow, only 33 meV below the CBM. This is because Sn has three more valence electrons than Cu. Two of them sit at the deep Sn 5*s* level and the other occupies the higher energy Sn 5*p* orbitals. As such, it is much easier to remove the first electron, which leads to the very shallow $Sn_{Cu}\epsilon(0/+)$ level, but it is much more difficult to remove the electron from the deep Sn 5*s* level, which is why $\epsilon(+/2+)$ and $\epsilon(2+/3+)$ of Sn_{Cu} are much deeper in the band gap. Therefore, these features are directly related to the stability of upper 4+ and lower 2+ oxidation states of Sn.[52] Similarly, by counting the number of valence electrons of Cu, Zn, and Sn, we can explain that (i) $\epsilon(0/+)$ is close to $\epsilon(+/2+)$ for Sn_{Zn}, (ii) the Sn_i level is close to the CBM when its charge state is less than 2+, but its $\epsilon(2+/3+)$ and $\epsilon(3+/4+)$ levels lie deep in the band gap.

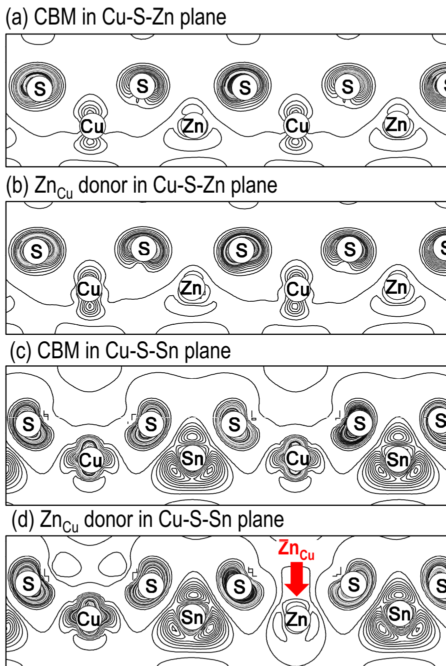

FIG. 6. (Color online) The contour plot of the charge density of the CBM state and Zn_{Cu} donor state in Cu-S-Zn and Cu-S-Sn planes, respectively. The red arrow shows the atomic site of the Zn_{Cu} antisite.

In Fig. 3, the formation-energy lines of acceptors such as Cu_{Zn} and V_{Cu} are always below those of donors, even when E_F is at the VBM, the charged donors Zn_{Cu}^{+} and Sn_{Zn}^{2+} have significantly lower formation energies than the neutral donors. This low acceptor formation energy explains the experimental observation by different groups that intrinsic Cu_2ZnSnS_4 samples always show *p*-type conductivity.[1,8,10,24–29] Due to the lowest formation energy of Cu_{Zn}, we can further attribute the *p*-type conductivity of Cu_2ZnSnS_4 to Cu_{Zn} antisite, different from the situation in $CuInSe_2$ where the *p*-type self-doping is attributed to the lower-energy V_{Cu}. Our calculated 0.12 eV transition-energy level of Cu_{Zn} above the VBM and the 1.5 eV band gap of Cu_2ZnSnS_4 single crystals can also be used to explain the experimentally observed photoluminescence spectrum with a peak at around 1.3 eV.[27,53] In contrast to the wide range of experimental studies of the defect levels in binary CdTe and ternary $CuInSe_2$, the characterization of defect levels in Cu_2ZnSnS_4 is so far very poor, partially because the synthesis of high-quality crystal with low-defect density is difficult and partially because the intense interest in this quaternary compound does not have a long history. We have listed the transition-energy levels within the band gap of possible intrinsic defects in Fig. 4, to compare with future experimental characterization.

A further consequence of the strong energetic preference for acceptor defects is the *n*-type doping difficulty of Cu_2ZnSnS_4. Since the formation energy of charged acceptors decreases as the Fermi energy shifts upward, at the chemical-potential point **A**, $\Delta H(Cu_{Zn},-1)$ becomes negative at $E_F=0.12$ eV and the ΔH of other charged acceptors becomes negative at E_F around 0.8 eV. In $CuInSe_2$, when Cu is rich $\Delta H(V_{Cu},-1)$ becomes negative at $E_F=0.83$ eV,[33] closer to that in Cu_2ZnSnS_4, because $\Delta H(V_{Cu},0)$ are similar in $CuInSe_2$ and Cu_2ZnSnS_4. The negative formation energy means these defects will form spontaneously, killing the free electrons and pinning the Fermi level if we want to move the Fermi level to close to the CBM and dope the sample *n* type.[32,33,54] Especially for the Cu_{Zn} antisite, it forms very easily when E_F deviates from the VBM and poses a more

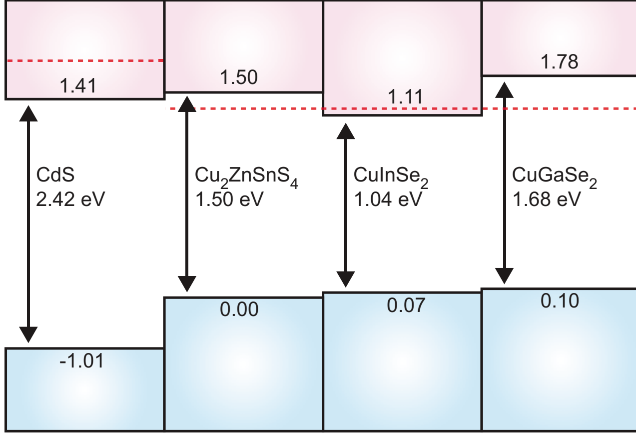

FIG. 7. (Color online) The band alignment between CdS, Cu_2ZnSnS_4, $CuInSe_2$, and $CuGaSe_2$ (the effects of spin-orbital coupling are included). The red (dashed) line near the CBM shows the pinning energy of Fermi level for n-type doping.

severe difficulty when doping n-type Cu_2ZnSnS_4 compared to $CuInSe_2$. This limit may be one negative factor limiting the performance of Cu_2ZnSnS_4 solar cells, e.g., the type inversion cannot form at the interface between absorber and window layers to facilitate efficient electron-hole separation.

The n-type doping difficulty can also be understood according to the band alignment of Cu_2ZnSnS_4, $CuInSe_2$, and $CuGaSe_2$, as shown in Fig. 7. Previous calculations have shown that the Fermi-level pinning energy for n-type doping in chalcopyrites is located at about 0.06 eV above the CBM of $CuInSe_2$,[54] so according to our calculated band offset between Cu_2ZnSnS_4 and $CuInSe_2$, the Fermi energy is pinned at 0.33 eV below the CBM of Cu_2ZnSnS_4, if we assume that it lines up for all chalcopyrite and kesterite compounds, since they have similar character in the electronic structure. The lineup of Fermi-level pinning energy indicates that the large band gap, thus the high CBM level of Cu_2ZnSnS_4 makes efficient n-type doping more difficult, similar to that in $CuGaSe_2$.

The small valence-band offset between Cu_2ZnSnS_4 and $CuInSe_2$ is somewhat unexpected, since usually sulfides have lower valence band than selenides due to their lower $3p$ level. However, in Cu_2ZnSnS_4, the S p-Zn d coupling is stronger than the Se p-In d coupling. Moreover, the lower p level and the smaller size of sulfur make the p-d hybridization between S and Cu stronger in Cu_2ZnSnS_4, pushing the VBM up relative to that in $CuInSe_2$ and thus reducing the band offset.

One important characteristic in the band alignment between CdS and Cu_2ZnSnS_4 is their type-II band offset, i.e., the CBM is lower on the CdS window layer and the VBM is higher on Cu_2ZnSnS_4 absorber layer (Fig. 7) which facilitates electron-hole separation, different from that for $CdS/CuInSe_2$ where a type-I offset is present.[55] It has been proposed that in $CdS/CuInSe_2$ solar cells, there is an ordered vacancy compound (OVC) layer such as $CuIn_3Se_5$ at the surface of the $CuInSe_2$ solar cells and this OVC layer has a type-II band lineup with respect to $CuInSe_2$. Band bending at the absorber layer benefits the electron-hole separation and is taken as one of the reasons for the good performance of $CuIn_{1-x}Ga_xSe_2$ cells according to device simulation.[17,56] Although a Cu_2ZnSnS_4-based OVC has not yet been observed, the type-II band lineup of CdS/Cu_2ZnSnS_4 can be a positive factor for achieving high conversion efficiencies in future CZTS solar-cell devices. These calculated band alignment results provide basic physical parameters, which are important for the device simulation and optimization process.[56]

C. Charge compensated defect complexes

One advantage of $CuInSe_2$ as a thin-film solar-cell absorber is its electrically benign character even with high degrees of nonstoichiometry and defect populations. This is due to the electronic passivation provided by the $[2V_{Cu}^{-}+In_{Cu}^{2+}]$ defect complex.[17] Since the quaternary kesterite material has more possible intrinsic defects, now we will study the complexes composed of the low-energy defects, to see if the same benign character is inherited in Cu_2ZnSnS_4.

1. Formation energy of defect complexes

According to the calculated formation energy of single defects at point **E** in Table I, Cu_{Zn}-, Cu_{Sn}-, Zn_{Sn}-, V_{Cu}-, and V_{Zn}-related defect complexes should have low formation energies, thus high probability to form in thermodynamic equilibrium. In Table II, we listed the formation energy of eight defect complexes, in which acceptors are charge compensated by the donors.

When the defects comprising these complexes are separated from each other without interaction, we define the formation energy $\Delta H_{separated}$ of noninteracting neutral defects as the sum of the formation energy of the two isolated single defects. The formation energy of defect complexes can be lowered considerably through the interaction when the defects bind, including contributions from: (i) charge compensation, i.e., the charge transfer from neutral donors to neutral acceptors; (ii) Coulomb attraction between charged donors and acceptors; and (iii) strain relief.[17] The first contribution could be as large as the band gap, i.e., 1.5 eV per electron for Cu_2ZnSnS_4, since the electron occupying the high donor

TABLE II. The calculated formation energy $\Delta H_{separated}=\Delta H(\alpha)+\Delta H(\beta)$ of noninteracting neutral defects α and β, the interaction ΔH_{int}, and the formation energy $\Delta H_{complex}$ (in eV) of the defect complexes $\alpha+\beta$ at chemical-potential point **E**, i.e., $\Delta H_{int}=\Delta H_{complex}-H_{separated}$.

Complexes	$V_{Cu}+Zn_{Cu}$	$V_{Zn}+Sn_{Zn}$	$Cu_{Zn}+Zn_{Cu}$	$Cu_{Sn}+Sn_{Cu}$	$Zn_{Sn}+Sn_{Zn}$	$Zn_{Sn}+2Zn_{Cu}$	$Cu_{Zn}+Cu_i$	$Zn_{Sn}+Zn_i$
$\Delta H_{separated}$	3.10	5.13	2.43	7.41	4.80	5.55	3.24	6.71
ΔH_{int}	−2.35	−3.68	−2.22	−5.42	−3.94	−4.69	−2.25	−4.64
$\Delta H_{complex}$	0.75	1.45	0.21	1.99	0.86	0.86	0.98	2.08

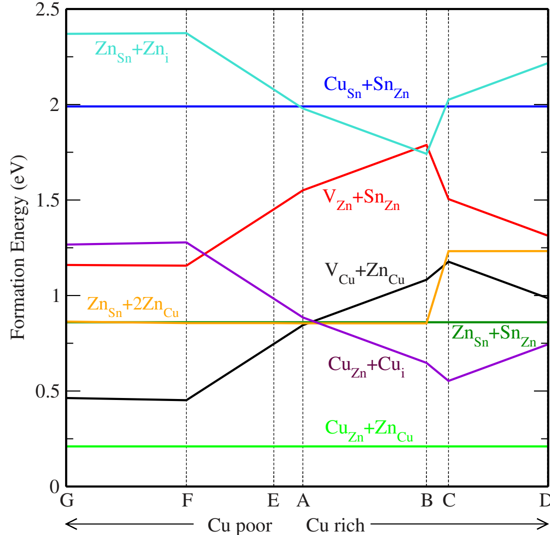

FIG. 8. (Color online) The formation energy of charge-compensated defect complexes in Cu_2ZnSnS_4 as a function of the chemical potential at points **A**, **B**, **C**, **D**, **E**, **F**, and **G** shown in Fig. 1 and Table I.

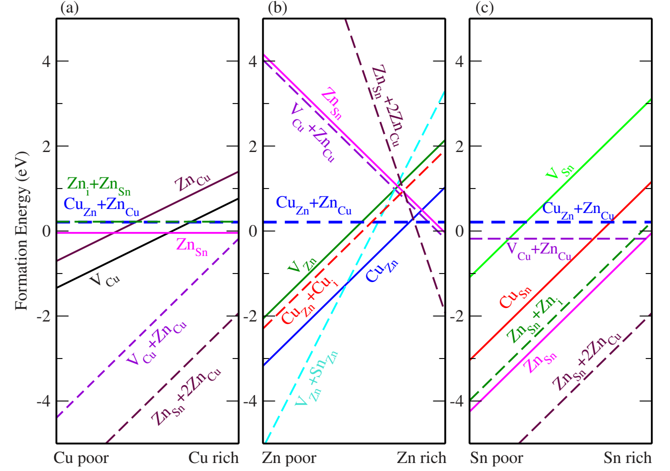

FIG. 9. (Color online) The formation energy $\Delta H(\alpha,0)$ of low-energy point defects and defect complexes in Cu_2ZnSnS_4 as a function of the chemical potential: (a) μ_{Cu} from −2.10 to 0 eV (Cu poor to rich), $\mu_{Zn}=0$, and $\mu_{Sn}=0$, (b) $\mu_{Cu}=0$, μ_{Zn} from −4.21 to 0 eV (Zn poor to rich), and $\mu_{Sn}=0$, and (c) $\mu_{Cu}=0$, $\mu_{Zn}=0$, and μ_{Sn} from −4.21 to 0 eV (Sn poor to rich). In contrast to Figs. 2 and 8, here the thermodynamic limits of secondary phase formation are excluded.

level near the CBM can transfer to the low-lying acceptor level near the VBM. In Table II, we have listed the different contributions to the formation energy of defect complexes: (i) $\Delta H_{separated}$ at chemical-potential point **E** and (ii) ΔH_{int} sums the three interactions when two defects get close. As we can see, the binding energy ΔH_{int} reduces the formation energy of complexes significantly, and the absolute value of ΔH_{int} depends on the band gap multiplied by defect charge, e.g., 1.5×1 eV for $[V_{Cu}^{-}+Zn_{Cu}^{+}]$, 1.5×2 eV for $[V_{Zn}^{2-}+Sn_{Zn}^{2+}]$, and 1.5×3 eV for $[Cu_{Sn}^{3-}+Sn_{Cu}^{3+}]$, which shows the charge compensation does play an important role in the pair interaction and there is an 1.5 eV energy gain when one electron leaves the donor level near the CBM and occupies the acceptor level near the VBM.

In our calculation of the defect complexes, we have considered different structural configurations of the complexes and present the results for the lowest-energy configurations. Due to charge compensation, or the charge transfer from donor to the acceptor, the defects forming the complex are charged, so the Coulomb interaction makes them attracted to each other and the most closely bound configuration always has the lowest energy.

$\Delta H_{complex}$ in Table II sums both the contribution $\Delta H_{separated}$ and ΔH_{int}, showing the probability of defect formation at the chemical-potential point **E**. The defect pair $[Cu_{Zn}^{-}+Zn_{Cu}^{+}]$ stands out as having the lowest $\Delta H_{complex}$. For defect pairs which involve atom exchange with the external reservoirs, their formation energy also depends on the chemical potential, such as $[V_{Cu}^{-}+Zn_{Cu}^{+}]$ and $[V_{Zn}^{2-}+Sn_{Zn}^{2+}]$, while those without atom exchange, such as $[Cu_{Zn}^{-}+Zn_{Cu}^{+}]$, have a formation energy independent of the chemical potential. In Fig. 8, we plot $\Delta H_{complex}$ as a function of the chemical potential along $\mathbf{G}\rightarrow\mathbf{F}\rightarrow\mathbf{E}\rightarrow\mathbf{A}\rightarrow\mathbf{B}\rightarrow\mathbf{C}\rightarrow\mathbf{D}$. The antisite pair $[Cu_{Zn}^{-}+Zn_{Cu}^{+}]$ has a formation energy (0.21 eV/pair) lower than all other complexes, showing this pair should have a high population in Cu_2ZnSnS_4 crystals. This antisite pair can also be taken as the occupational exchange between Cu and Zn crystallographic sites, which explains Cu and Zn partial disorder in Cu_2ZnSnS_4 samples observed using neutron scattering.[12,44]

Other pairs besides $[Cu_{Zn}^{-}+Zn_{Cu}^{+}]$ have relatively high formation energy along the **G** to **D** line, so their formation should be limited in stoichiometric samples, but when the samples are of poor quality like in sputtered thin films, their formation energy may decrease depending on the chemical potential. In Fig. 9, we plot the formation-energy change in low-energy defects and complexes along $\mu_{Cu}=0$, $\mu_{Zn}=0$, and $\mu_{Sn}=0$ axes in the chemical-potential landscape, to show the most probable defect configuration at different growth condition, although these lines are excluded to avoid the formation of secondary phases. It is clear that the formation energy of some complexes changes more rapidly as the chemical potential changes, making them the lowest-energy defect when a certain element is extremely rich or poor. For example, the change in slope of $[V_{Cu}^{-}+Zn_{Cu}^{+}]$ and $[Zn_{Sn}^{2-}+2Zn_{Cu}^{+}]$ as a function of μ_{Cu} is two times as large as that of the isolated V_{Cu} or Zn_{Cu} defects, which can be understood according to Eq. (1) and the more atom exchange of defect complexes with the external reservoir. From Fig. 9 we can see, $[V_{Cu}^{-}+Zn_{Cu}^{+}]$, $[Zn_{Sn}^{2-}+2Zn_{Cu}^{+}]$, and $[V_{Zn}^{2-}+Sn_{Zn}^{2+}]$ are the three lowest energy complexes if the Cu, Zn, or Sn chemical potentials are extremely rich or poor, and the resulting samples deviate seriously from their formal stoichiometry.

2. Electronic passivation of defect complexes

In $CuInSe_2$, the $[2V_{Cu}^{-}+In_{Cu}^{2+}]$ complex plays an important role in the electronic passivation of the In_{Cu} deep donor level. In Cu_2ZnSnS_4, there are more deep levels caused by the intrinsic defects as we have demonstrated, and when the sample is seriously nonstoichiometric, some of them may exist, acting as traps of free carriers or recombination cen-

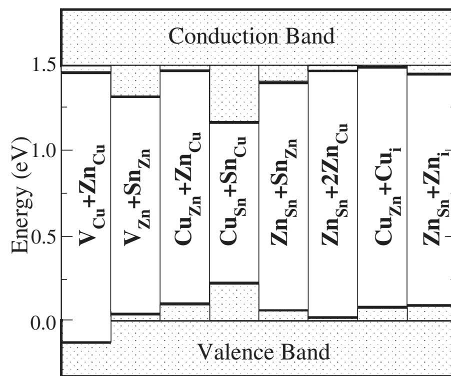

FIG. 10. The CBM and the VBM levels (in eV) of Cu_2ZnSnS_4 with different charge-compensated defect complexes relative to the host material at 0 eV and 1.5 eV, respectively.

ters, which reduces the efficiency of solar-cell devices. For example, in *p*-type samples, some charged donors may form and produce deep levels in the band gap. In the following paragraph, we will discuss if the formation of defect complexes may passivate the deep levels in Cu_2ZnSnS_4 and its influence on the solar-cell performance.

In Fig. 10, we plot the CBM and the VBM shift caused by different defect complexes. Charge compensation between donors and acceptors pushes the single-electron donor level up and the single-electron acceptor level down. For example, the Zn_{Cu} level is pushed up by 0.07 eV when the $[Cu_{Zn}^{1-}+Zn_{Cu}^{1+}]$ pair is formed, and the deep Sn_{Cu} level is pushed up by 0.42 eV when $[Cu_{Sn}^{3-}+Sn_{Cu}^{3+}]$ pair is formed. When there are charged donor defects, they usually have high formation energy, e.g., $\Delta H(Sn_{Cu},+3)=3.31$ eV with E_F at the VBM, but if a $[Cu_{Sn}^{3-}+Sn_{Cu}^{3+}]$ pair forms, its formation energy drops to only 1.99 eV, so the pair will readily form when the single donor exists and eliminates the deep levels. As we can see, in this quaternary semiconductor there are more defect complexes due to the increased chemical freedom, thus electronic passivation is more probable, which indicates Cu_2ZnSnS_4 thin-film solar cells may also possess the same electrically benign character as $CuInSe_2$. This type of self-compensation is expected to be a general feature of other I_2-II-IV-VI_4 semiconductors.[13]

V. CONCLUSIONS

In conclusion, the defect properties of the quaternary Cu_2ZnSnS_4 semiconductor have been systematically studied using first-principles calculations. We have found that: (i) chemical-potential control is very important in growing good-quality crystals with no secondary phase formation and low-defect density. (ii) The observed *p*-type conductivity comes mainly from the Cu_{Zn} antisite with a relatively deeper acceptor level compared to the Cu vacancy in ternary chalcopyrites. (iii) The low formation energy of acceptor defects makes *n*-type doping difficult in Cu_2ZnSnS_4. (iv) The band alignment for CdS/Cu_2ZnSnS_4 is type II, different from that for $CdS/CuInSe_2$. (v) Charge-compensated defect complexes are easy to form and passivate the deep donor levels, which may give rise to electrically benign character in thin-film Cu_2ZnSnS_4 solar cells. Some features of the defect physics of Cu_2ZnSnS_4 are expected to be common in other quaternary I_2-II-IV-VI_4 semiconductors.

ACKNOWLEDGMENTS

The work in Fudan is supported by the National Sciences Foundation of China (Grants No. 10934002 and No. 1095011032), the Research Program of Shanghai municipality and MOE, the Special Funds for Major State Basic Research. S.C. is supported by NSF of Shanghai (Grant No. 10ZR1408800) and NSF of China (Grants No. 60990312). A.W. would like to acknowledge funding from the European Union. The work at NREL is funded by the U.S. Department of Energy, under Contract No. DE-AC36-08GO28308.

[1] N. Nakayama and K. Ito, Appl. Surf. Sci. **92**, 171 (1996).
[2] K. Tanaka, M. Oonuki, N. Moritake, and H. Uchiki, Sol. Energy Mater. Sol. Cells **93**, 583 (2009).
[3] A. Weber, S. Schmidt, D. Abou-Ras, P. Schubert-Bischoff, I. Denks, R. Mainz, and H. W. Schock, Appl. Phys. Lett. **95**, 041904 (2009).
[4] Q. Guo, H. W. Hillhouse, and R. Agrawal, J. Am. Chem. Soc. **131**, 11672 (2009).
[5] S. C. Riha, B. A. Parkinson, and A. L. Prieto, J. Am. Chem. Soc. **131**, 12054 (2009).
[6] C. Steinhagen, M. G. Panthani, V. Akhavan, B. Goodfellow, B. Koo, and B. A. Korgel, J. Am. Chem. Soc. **131**, 12554 (2009).
[7] C. Sevik and T. Çağin, Appl. Phys. Lett. **95**, 112105 (2009).
[8] J. J. Scragg, P. J. Dale, L. M. Peter, G. Zoppi, and I. Forbes, Phys. Status Solidi B **245**, 1772 (2008).
[9] H. Katagiri, K. Jimbo, W. S. Maw, K. Oishi, M. Yamazaki, H. Araki, and A. Takeuchi, Thin Solid Films **517**, 2455 (2009).
[10] Y. B. Kishore Kumar, G. S. Babu, P. U. Bhaskar, and V. S. Raja, Sol. Energy Mater. Sol. Cells **93**, 1230 (2009).
[11] A. Weber, H. Krauth, S. Perlt, B. Schubert, I. Kötschau, S. Schorr, and H. Schock, Thin Solid Films **517**, 2524 (2009).
[12] S. Chen, X. G. Gong, A. Walsh, and S.-H. Wei, Appl. Phys. Lett. **94**, 041903 (2009).
[13] S. Chen, X. G. Gong, A. Walsh, and S.-H. Wei, Phys. Rev. B **79**, 165211 (2009).
[14] J. Paier, R. Asahi, A. Nagoya, and G. Kresse, Phys. Rev. B **79**, 115126 (2009).
[15] J. Scragg, P. Dale, and L. Peter, Thin Solid Films **517**, 2481 (2009).
[16] T. K. Todorov, K. B. Reuter, and D. B. Mitzi, Adv. Mater. (to be published).
[17] S. B. Zhang, S.-H. Wei, A. Zunger, and H. Katayama-Yoshida, Phys. Rev. B **57**, 9642 (1998).
[18] S.-H. Wei and S. B. Zhang, J. Phys. Chem. Solids **66**, 1994 (2005).
[19] S.-H. Wei, S. B. Zhang, and A. Zunger, Appl. Phys. Lett. **72**,

3199 (1998).
[20] S. Lany and A. Zunger, Phys. Rev. Lett. **100**, 016401 (2008).
[21] S. Chen, X. G. Gong, A. Walsh, and S.-H. Wei, Appl. Phys. Lett. **96**, 021902 (2010).
[22] J. M. Raulot, C. Domain, and J. F. Guillemoles, J. Phys. Chem. Solids **66**, 2019 (2005).
[23] A. Nagoya, R. Asahi, R. Wahl, and G. Kresse, Phys. Rev. B **81**, 113202 (2010).
[24] K. Tanaka, T. Nagatomo, D. Kawasaki, M. Nishio, Q. Guo, A. Wakahara, A. Yoshida, and H. Ogawa, J. Phys. Chem. Solids **66**, 1978 (2005).
[25] R. A. Wibowo, W. S. Kim, E. S. Lee, B. Munir, and K. H. Kim, J. Phys. Chem. Solids **68**, 1908 (2007).
[26] Y. Miyamoto, K. Tanaka, M. Oonuki, N. Moritake, and H. Uchiki, Jpn. J. Appl. Phys. **47**, 596 (2008).
[27] M. Altosaar, J. Raudoja, K. Timmo, M. Danilson, M. Grossberg, J. Krustok, and E. Mellikov, Phys. Status Solidi A **205**, 167 (2008).
[28] M. Grossberg, J. Krustok, K. Timmo, and M. Altosaar, Thin Solid Films **517**, 2489 (2009).
[29] K. Oishi, G. Saito, K. Ebina, M. Nagahashi, K. Jimbo, W. S. Maw, H. Katagiri, M. Yamazaki, H. Araki, and A. Takeuchi, Thin Solid Films **517**, 1449 (2008).
[30] X. Zhang, X. Shi, W. Ye, C. Ma, and C. Wang, Appl. Phys. A: Mater. Sci. Process. **94**, 381 (2009).
[31] K. Hönes, E. Zscherpel, J. Scragg, and S. Siebentritt, Physica B **404**, 4949 (2009).
[32] S.-H. Wei and S. B. Zhang, Phys. Rev. B **66**, 155211 (2002).
[33] C. Persson, Y.-J. Zhao, S. Lany, and A. Zunger, Phys. Rev. B **72**, 035211 (2005).
[34] M. A. Contreras, K. Ramanathan, J. AbuShama, F. Hasoon, D. L. Young, B. Egaas, and R. Noufi, Prog. Photovoltaics **13**, 209 (2005).
[35] R. Schurr *et al.*, Thin Solid Films **517**, 2465 (2009).
[36] T. Todorov, M. Kita, J. Carda, and P. Escribano, Thin Solid Films **517**, 2541 (2009).
[37] A. Weber, R. Mainz, and H. W. Schock, J. Appl. Phys. **107**, 013516 (2010).
[38] S.-H. Wei, Comput. Mater. Sci. **30**, 337 (2004).
[39] G. Kresse and J. Furthmuller, Phys. Rev. B **54**, 11169 (1996).
[40] J. P. Perdew, J. A. Chevary, S. H. Vosko, K. A. Jackson, M. R. Pederson, D. J. Singh, and C. Fiolhais, Phys. Rev. B **46**, 6671 (1992).
[41] G. Kresse and D. Joubert, Phys. Rev. B **59**, 1758 (1999).
[42] J. Heyd, G. E. Scuseria, and M. Ernzerhof, J. Chem. Phys. **118**, 8207 (2003).
[43] J. Paier, M. Marsman, K. Hummer, G. Kresse, I. C. Gerber, and J. G. Ángyán, J. Chem. Phys. **124**, 154709 (2006).
[44] S. Schorr, H. J. Hoebler, and M. Tovar, Eur. J. Mineral. **19**, 65 (2007).
[45] S.-H. Wei and A. Zunger, Appl. Phys. Lett. **72**, 2011 (1998).
[46] S. Chen, X. G. Gong, and S.-H. Wei, Phys. Rev. B **75**, 205209 (2007).
[47] Y.-H. Li, A. Walsh, S. Chen, W.-J. Yin, J.-H. Yang, J. Li, J. L. F. D. Silva, X. G. Gong, and S.-H. Wei, Appl. Phys. Lett. **94**, 212109 (2009).
[48] R. W. G. Wyckoff, *Crystal Structures*, 2nd ed. (Wiley, New York, 1963), Vol. 1.
[49] M. Onoda, X.-A. Chen, A. Sato, and H. Wada, Mater. Res. Bull. **35**, 1563 (2000).
[50] K. Sekiguchi, K. Tanaka, K. Moriya, and H. Uchiki, Phys. Status Solidi C **3**, 2618 (2006).
[51] H. Katagiri, Thin Solid Films **480-481**, 426 (2005).
[52] A. Walsh and G. W. Watson, Phys. Rev. B **70**, 235114 (2004).
[53] K. Tanaka, Y. Miyamoto, H. Uchiki, K. Nakazawa, and H. Araki, Phys. Status Solidi A **203**, 2891 (2006).
[54] S. B. Zhang, S.-H. Wei, and A. Zunger, J. Appl. Phys. **83**, 3192 (1998).
[55] S.-H. Wei and A. Zunger, Appl. Phys. Lett. **63**, 2549 (1993).
[56] A. Bouloufa, K. Djessas, and A. Zegadi, Thin Solid Films **515**, 6285 (2007).